



Estimation of Amazon River discharge based on EOF analysis of GRACE gravity data



Jooyoung Eom^a, Ki-Weon Seo^{b,*}, Dongryeol Ryu^c

^a Unit of Ice Sheet and Sea Level Changes, Korea Polar Research Institute, Incheon 21990, Republic of Korea

^b Department of Earth Science and Education, Seoul National University, Seoul 08826, Republic of Korea

^c Department of Infrastructure Engineering, University of Melbourne, Parkville, Victoria 3010, Australia

ARTICLE INFO

Article history:

Received 29 April 2016

Received in revised form 6 January 2017

Accepted 12 January 2017

Available online 20 January 2017

Keywords:

GRACE

River discharge

Empirical Orthogonal Function

Amazon basin

ABSTRACT

River discharge is a critical component for understanding hydrological processes and sustainable management of water resources. The importance of discharge observation has increased due to its potential extreme variation resulting from the projected climate change and stronger variability of precipitation and temperature in some large basins. However, inherent difficulties in ground-based observations and decreasing number of gauge stations hinder accurate measurement of global river discharge and its spatio-temporal variations. Various remote sensing methods have been examined as alternatives, however, they require ground measurements to convert their proxy measurements into the actual river discharge. In this study, we estimate the discharge at the Óbidos station and the mouth of the Amazon basin using the water storage variations derived from GRACE gravity data without relying on any auxiliary ground observations. We extract the water mass signal along the main stem of the river by applying the Empirical Orthogonal Function (EOF) for water storage variations over the basin. The relative water storage variations along the main stem derived from the EOF decomposition are highly correlated with in-situ discharge at the Óbidos. However, in high water season, the GRACE-based discharge is estimated larger than the in-situ observations, and the difference is particularly significant during the 2009 extreme flood season. We argue that the in-situ river discharge in 2009 was underestimated due to the missed water volume for the flow detouring around the Óbidos gauge station during the high-flow event. Net river discharge of the Amazon Basin to Atlantic Ocean is also estimated, and its annual discharge is about 23% larger than that of the Óbidos. In particular, 2009 river discharge to Atlantic Oceans is estimated as 1050 Gton.

© 2017 Elsevier Inc. All rights reserved.

1. Introduction

Continuous monitoring of river discharge is essential to understand the hydrological cycle and to manage water resources and hydrological disasters (Hersch, 2009; IPCC, 2014). Its variation with inter-annual and longer time scales is also an integrated measure of global and regional climate and hydrological changes (Knutti et al., 2004; Milly et al., 2002; Nohara et al., 2006; Richey et al., 1989; Shabalova et al., 2003). Discharge is usually measured across the stream at gauge stations with Acoustic Doppler Current Profiler (ADCP), which uses sound waves to calculate current velocity profiles and water depth (Kostaschuk et al., 2004; Simpson and Oltmann, 1993). However, limitations of ADCP, such as high cost and difficulty of field experiment, often make frequent and automated discharge measurements infeasible particularly for large rivers with complex flow paths. To acquire

continuous time series of river discharge at in-situ stations, continuously measured water level data are converted to discharge using the regression analysis of an empirical relationship between discharge and water level data called the rating curve. Based on the empirical relationship represented by the rating curve, river discharge can be indirectly 'estimated' from water level observations.

However, the empirical relationship naturally varies over time due to the geomorphological changes of river base by erosion and deposition (Jalbert et al., 2011). In addition, intermittent development of new floodplain and formation of episodic braided channels in flood season further increase the uncertainty of the rating curve analysis (Alsdorf and Lettenmaier, 2003; Di Baldassarre and Claps, 2010; Di Baldassarre and Montanari, 2009; Leonard et al., 2000). This is particularly true for the Amazon River because significant amount of water can flow outside the poorly defined main river channel during flooding. Therefore, it is difficult to estimate discharge during extreme floods, such as the recent one occurred in the austral summer of 2009 (Filizola et al., 2014). Furthermore, there exists additional uncertainty in the empirical relationship for such high-record events because the 'extreme' events are

* Corresponding author.

E-mail address: seokiweon@snu.ac.kr (K.-W. Seo).

inherently represented by a small number of samples and, furthermore, the measurements are often limited for safety reasons (Lang et al., 2010; Petersen-Overleir and Reitan, 2009).

As an alternative approach, satellite remote sensing has been applied for estimating river discharge (Alsdorf and Lettenmaier, 2003). For rivers with well-established rating curves, remote observations of water surface height can yield estimations of discharge from the empirical relationship. Kouraev et al. (2004) and Zakharova et al. (2006) used water heights derived from satellite altimetry to determine discharge in the Ob and the Amazon basins, respectively. Getirana et al. (2009) combined spatial altimetry data with a hydrologic model (MGB-IPH) to estimate discharge over the Northern Amazon basin and De Paiva et al. (2013) evaluated performance of MGB-IPH by comparing the model discharge with the satellite altimetry data and terrestrial water storage (TWS) changes from the Gravity Recovery and Climate Experiment (GRACE) mission over the Amazon River basin. Satellite imagery methods based on optical, infrared and microwave radar imagery (e.g., Moderate Resolution Imaging Spectroradiometer (MODIS), Landsat and European Remote Sensing-synthetic aperture radar (ERS-SAR)) are able to determine horizontal water extent that forms the boundaries between water and land, and in turn can produce water height in combination with high-resolution digital elevation model (Smith, 1997; Xu et al., 2004). The imagery method is useful for rivers in which discharge changes are relatively insensitive to water height variation as in braided or temporarily flooded channels. In this case, water extent vs. discharge rating curve is necessary to estimate discharge from water extent (Smith, 1997). All the methods reviewed so far require similar empirical relationship between water surface geometry (height or extent) and discharge (Leon et al., 2006). Therefore, those satellite-based discharge estimation methods are also constrained by the availability of the in-situ observation and accurate digital elevation model (Alsdorf et al., 2007; Bjerklie et al., 2003). Recently, attempts have been made to estimate river discharge based on satellite remote sensing without in-situ data (Gleason and Smith, 2014; Negrel and Kosuth, 2012), yet those results are limited to recover variations of in-situ data, particularly during the high water seasons.

River discharge estimation based on satellite gravity observations offers an alternative method that does not require a priori empirical relationship because it uses the gravity changes induced by water mass variations that has a direct association with discharge. Syed et al. (2005) estimated discharge from the Amazon and the Mississippi basins based on water storage variations observed by the GRACE time-varying gravity in combination with precipitation and evapotranspiration computed from the European Centre for Medium-Range Forecasts (ECMWF) operational forecast analyses. They combined them in a water balance equation (WBE) for river discharge (R_t) estimate as:

$$R_t = P_t - E_t - \frac{\partial S_t}{\partial t}, \quad (1)$$

where P_t and E_t are accumulation of precipitation and evapotranspiration, respectively, and ∂S_t is water storage variations over the whole basin with the time period ∂t of one month for applying to GRACE estimates. However, this method is susceptible to the errors in precipitation and evapotranspiration from the meteorological model that typically involves fairly large uncertainties, and time-derivative term of water storage in WBE can cause cumbersome random noise (Sheffield et al., 2009). Consequently, the WBE-based methods with external forcing variables resulted in large discrepancies between in-situ data and estimated river discharge data (Syed et al., 2005).

On the other hand, Riegger and Tourian (2014) showed that there is a constant time delay between variabilities in basin-wide water storage and river runoff, indicating that discharge can be estimated via total water storage variations from GRACE and vice versa. Since the time delay between discharge and total water storage is caused by the transition time from storage to runoff through a basin (Riegger and Tourian,

2014), water storage variations confined to a main stem is likely in-phase with discharge variations and useful for discharge estimate. Therefore, this study explores a method to estimate river discharge in the Amazon River basin using water storage changes along the main stem as a complementary in-situ gauge sampling.

In this study, we extract water storage changes along the main stem of river using the Empirical Orthogonal Function (EOF) technique. The EOF method is effective in separating error and signal of the GRACE data (Wouters and Schrama, 2007) due to its capacity of finding spatial correlation in spatio-temporal data (Navarra and Simoncini, 2010). The water mass signal along the main stem recovered from the EOF analysis (denoted by GRACE-EOF hereafter) may include not only the water storage variation in the main stem, which is related with river discharge, but also various water balance components near the main stem, such as surface runoff, soil moisture and groundwater. However, in the Amazon River basin, the phase difference between the river storage and the other water balance components is known to be shorter than a month near the main stem (Alsdorf et al., 2010). As a result, water storage variations on the main stem recovered from GRACE-EOF can be assumed to represent the temporal variability very similar to the river storage and consequently be used to estimate river discharge variation.

2. Data and method

2.1. In-situ data for river discharge

We select the Óbidos station for the Amazon River discharge observation point, which is operated by the ORE-HYBAM project (www.ore-hybam.org). In-situ data from the station is available since 1968. The Óbidos station is the nearest gauge station on the main stem to the mouth of the basin, although it is located approximately 800 km upstream from the outlet. The basin area above the Óbidos station is estimated to comprise 80% of the whole Amazon Basin, and about 90% of precipitation is captured in this basin area (Zeng et al., 2008). The Tapjos and the Xingu Rivers, which are confluents with main stem below Óbidos, contribute only 10% of water to total mean discharge. Therefore, many hydrologic studies on the Amazon basin have used hydrometric data observed at the Óbidos station (Espinoza et al., 2009; Frappart et al., 2013; Marengo, 2005; Marengo et al., 2012; Yoon and Zeng, 2010).

2.2. GRACE monthly gravity solutions

To investigate water mass change, monthly GRACE solutions, determined by the Center for Space Research (CSR), University of Texas at Austin, are used in this study. The latest release (RL05) of GRACE Level-2 data consists of fully normalized spherical harmonics (SH) gravity coefficients up to degree and order 60, equivalent to a spatial resolution of around 3–400 km (Bettadpur, 2012). We use 124 monthly datasets from January 2003 to December 2013, and interpolate linearly for 8 missing months (Jun 2003; Jan and Jun 2011; May and Oct 2012; Mar, Aug and Sep 2013) in SH domain, yielding 132 monthly time-series for 11 years. Due to the previously reported unreliability, the degree-2 zonal harmonic (C20) coefficients are replaced with results from Satellite Laser Ranging (SLR) observation (Cheng and Tapley, 2004). Post-glacial rebound (PGR) effects are corrected by the ICE-5G PGR model (A. et al., 2013). Peculiar north-south patterns in GRACE gravity solutions are parameterized by a polynomial fitting and removed from GRACE gravity solutions (Swenson and Wahr, 2006). Finally, surface mass change at latitude and longitude grid with 0.5° interval in terms of equivalent water thickness (EWT) (Wahr et al., 1998) is computed from the reduced SH. Since gravity variations associated with tides, atmospheric pressure and ocean bottom pressure are corrected during the determination of GRACE gravity solutions, resulting EWT over the Amazon basin nominally includes surface water in river, lake, floodplain and subsurface water in soil and aquifer.

2.3. Rotated EOF method

The EWT fields from the reduced GRACE SH data are still contaminated by the residual noise, which is commonly removed by Gaussian spatial smoothing (Klees et al., 2008; Schmidt et al., 2008; Tamisiea et al., 2007). However, the spatial averaging filters can cause signal loss, termed ‘leakage error’ (Longuevergne et al., 2010; Swenson and Wahr, 2002). Moreover, after the spatial filtering, the spatial resolution of the EWT field decreases, and this makes it difficult to identify water mass signal of main stem. The EOF analysis is an alternative method for GRACE data to separate signals from noise without diminishing the spatial resolution (Wouters and Schrama, 2007).

The time-varying EWT fields over the Amazon basin can be rearranged into a single matrix \mathbf{D} with size $n \times p$, in which n and p are numbers of temporal samplings and grids, respectively. In the EOF analysis, \mathbf{D} is decomposed into separate modes that are orthogonal to each other using the singular value decomposition (SVD) (Jolliffe, 2002);

$$\mathbf{D} = \mathbf{U}\mathbf{S}\mathbf{V}^T \quad (2)$$

where \mathbf{V} and \mathbf{U} are orthogonal matrices with size $n \times n$ and $p \times p$ respectively. The i th column vector of \mathbf{V} represents the i th mode spatial pattern of the dataset and is usually named EOF_i . Similarly, the i th column vector \mathbf{U} (named PC_i) shows temporal variations of the i th mode spatial pattern. \mathbf{S} is a rectangular diagonal matrix with size of $n \times p$, and their elements on the main diagonal are singular values of \mathbf{D} . The explained variance (EV) of the i th mode is calculated as:

$$EV = \sigma_i^2 / \sum_{k=1}^N \sigma_k^2 \times 100\%, \text{ where } N = \min(n, p). \quad (3)$$

Frappart et al. (2013) attempted to explain each mode as a corresponding hydraulic parameter, such as surface runoff, groundwater flow and water storage of floodplain. However interpretation of each mode should be made with caution since the hydraulic components can be correlated with each other in a given basin (Alsdorf et al., 2010), and thus a particular hydraulic component cannot be accounted for solely by a single EOF. This is because the 1st EOF mode is estimated to represent a spatio-temporal pattern with the maximum EV, and the 2nd mode is simply determined to be the largest EV among many modes orthogonal to the first one. Subsequent modes are also selected by similar ways. Furthermore, water storage variations in basins are not stationary. For example, a spatial pattern of water storage variation migrates northward over the Amazon basin through a year. Therefore, a particular hydraulic component tends to be projected on several modes, and similarly one mode can include water storage variations forced by various hydrologic components. This restriction is also true for extracting river discharge signal that is confined along and around river channels. The signal is expected to project into many EOF modes, and thus interpretation of river discharge from a single EOF mode possibly causes additional uncertainty.

This EOF limitation can be addressed in part by rotating vectors \mathbf{v} in \mathbf{V} matrix to construct new EOF modes,

$$\mathbf{W} = \mathbf{W}_s\mathbf{R}, \text{ with } \mathbf{V}_s = [\mathbf{v}_1, \mathbf{v}_2, \dots, \mathbf{v}_s], \quad (4)$$

in which \mathbf{R} is the rotation matrix and s is the number of EOF modes that are assumed to be signal, based on the variance fraction \mathbf{S} in Eq. (2). This modified version is called rotated EOF (REOF). Criterion of the rotation is to find a new EOF mode (\mathbf{W}) that is aligned with the direction of maximum variance in a given grid point: this is equivalent to finding the minimum number of new EOF modes that are sufficient to synthesize the original values of a grid point. In other words, REOF finds a mode to maximize the variance of certain grid points that are nearly zero in other modes while EOF maximizes the EV of a mode over a given domain. For example, the water mass signal along a river channel that

was projected into many EOF modes are re-projected to a single mode, and this new EOF mode has the maximum variance associated with the signal from the channel.

There are several different cost functions to maximize the variance. In this study, we use the VARIMAX method that is most widely used (Hannachi et al., 2007). The cost function is

$$f(\mathbf{w}_1, \mathbf{w}_2, \dots, \mathbf{w}_s) = \sum_{k=1}^s \left[p \sum_{i=1}^p w_k^i{}^4 - \left(\sum_{i=1}^p w_k^i{}^2 \right)^2 \right], \quad (5)$$

where w_k^i are the i th grid-point value of the k th REOF spatial pattern (REOF $_k$). The rotation angles are iteratively adjusted until the cost function is converged.

2.4. Synthetic GRACE data

To verify the use of GRACE-REOF to estimate the Amazon River discharge, it is necessary to test the method with synthetic GRACE data for which the ‘truth’ discharge is known. The GRACE gravity solutions over land include terrestrial water storage (TWS) changes reflecting the mass variations of soil moisture, groundwater, snow (and ice), lakes and water flow on river channels and floodplain (Cazenave and Chen, 2010). To simulate those TWS variations, model outputs from Global Land Data Assimilating System (GLDAS) (Rodell et al., 2004) with Noah land surface model is used. GLDAS incorporates data assimilations of four different model outputs. GLDAS/Noah is known to provide soil water storage similar to the annual cycle of GRACE estimates (Han et al., 2009).

The changes of total TWS for the Amazon basin can be partitioned into soil moisture and surface water storage components (Han et al., 2010). The soil moisture is simply given by the monthly GLDAS/Noah outputs at each 1-degree grid cell. The surface water storage represents mass variations associated with horizontal water transport through rivers and floodplains, but this component is not modeled in the GLDAS because the system mainly focuses on the vertical water fluxes. To simulate the lateral redistribution of water, a runoff routing method based on a continuity equation (OkI et al., 1999) is used. This routing method uses linear relationship between surface water storage and runoff, and thus runoff at river channel (i.e., synthetic ‘true’ discharge to be compared with the ‘estimated’ discharge from synthetic GRACE data) can be simulated by scaling of corresponding surface water storage. Han et al. (2010) solved the continuity equation for runoff routing in a spectral domain within seasonal frequency band to examine annual variations of surface water storage over the Amazon basin. In this study, the surface water storage is simulated by the spectral routing method (Han et al., 2010), but a complete set of spectra less than the Nyquist frequency is used to construct the broadband runoff time series at each grid cell. Three-hourly surface and subsurface runoff data from the GLDAS/Noah are incorporated as input parameters for the continuity equation, and simulated runoff time series at each grid cell and the soil moisture variations from the GLDAS/Noah are aggregated into total TWS over the basin.

Since the real GRACE data is contaminated by errors, it is necessary to incorporate the TWS and GRACE errors in the synthetic GRACE-REOF experiment. Errors in the monthly GRACE solutions are mainly attributed to the measurement noise and the aliasing error from unmodeled atmospheric and oceanic effects (Wahr et al., 2006). Those errors can be suppressed significantly by a spatial averaging because they are dominant over shorter wavelengths (Han et al., 2005; Seo and Wilson, 2005; Wahr et al., 2006). Therefore, differences between the real GRACE and its smoothed gravity solution may represent the GRACE error fields (Seo et al., 2015; Velicogna and Wahr, 2013). However, the difference between smoothed and unsmoothed GRACE data may also originate from true gravity variations since smoothing can diminish signals. Therefore, the residual mass variations from the

difference over the Amazon basin are highly correlated with the simulated TWS changes, and thus the correlated component are removed from the differences for the GRACE error estimate. Finally, the TWS changes from soil moisture and runoff and the estimated GRACE errors are combined to produce the synthetic GRACE data.

To examine similarity between synthetic and real GRACE data in spectral domain, we calculate degree amplitudes, which are the root-mean-squared of SH coefficients (for details, see equations (2) and (3) of Seo and Wilson (2005)). Fig. 1 shows degree amplitudes for the real (black) and synthetic (green) GRACE data over the Amazon basin during the study period from 2003 to 2013. The degree amplitudes for TWS and estimated error are also exhibited in blue and red lines, respectively. The green line (degree amplitude of synthetic GRACE data) shows two peaks around degrees 8 and 57. The peaks at lower and higher degrees are associated with TWS signal (blue) and GRACE error (red), respectively. In addition, the black line is close to the green line, and it indicates that synthetic GRACE data reproduces the real GRACE data reasonably over the study area. Comparisons between synthetic and real GRACE data in spatio-temporal domain are also made in EOF analysis below.

3. Results

3.1. Recovering river discharge from the synthetic data

The synthetic GRACE data are reduced by the conventional GRACE data procedures introduced in Section 2.2 except the PGR correction. The PGR effect is negligible in low latitude, and thus it was not included in the synthetic GRACE data. Reduced synthetic GRACE data are converted into 0.5° grid data, and then decomposed into EOF modes over the upstream of the Óbidos station in the Amazon basin using Eq. (2). Figs. 2a and b exhibit the spatial patterns of the first two modes ($EOF1-2$), and solid red and dashed blue lines in Fig. 2c show their corresponding time series ($PC1-2$). In Figs. 2a and b, the Amazon basin is bounded in the thick black line, and a main channel and major tributaries are mapped by thin black lines. The grey line marks the eastern boundary of the Óbidos sub-basin whose discharge has been continuously gauged at the Óbidos station (cyan triangle). The “ExVar” above each panel denotes the EV of the corresponding EOF mode in Eq. (3).

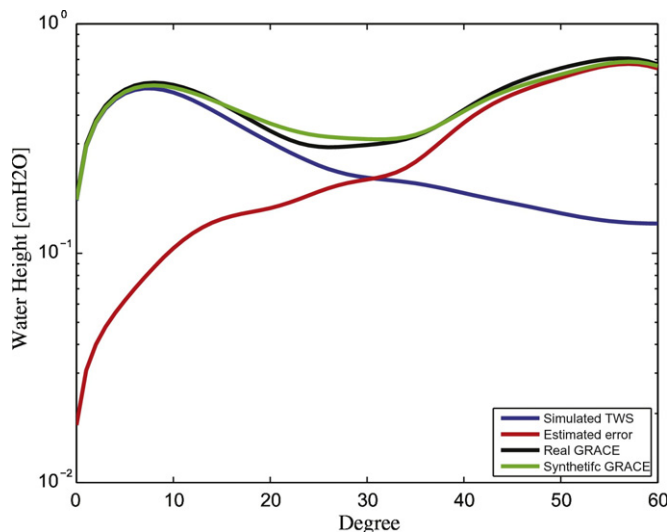


Fig. 1. Degree amplitudes for real and synthetic GRACE data. The synthetic GRACE data are shown in green, sum of the simulated TWS (blue) and estimated error (red). The degree amplitude for the real GRACE data shown in black agrees well with the synthetic GRACE data.

The first two modes account for 72.8% of the total variance, which implies that the simulated TWS changes in the basin can be largely represented by the first two modes. The black line in Fig. 2c shows synthetic river discharge variations at the Óbidos station. All time series in Fig. 2c are normalized by its standard deviation.

The 1st mode shows the largest apparent anomaly along the main stem (Fig. 2a, $EOF1$) while non-negligible anomaly is also observed over the entire basin. This indicates that the 1st mode includes signals associated with discharge on the main stem and other hydraulic components. To understand this further, $EOF1$ and $EOF2$ are compared with routed river flow and soil moisture variations in synthetic GRACE data. Figs. 3a and b show root mean squared (RMS) amplitudes of routed river flow and soil moisture variations in synthetic GRACE data. They are smoothed to be comparable with GRACE spatial resolution. To compare them with $EOF1$ and $EOF2$, the two modes are reconstructed, and their RMSs are shown in Figs. 3c and d, respectively. The RMS map of $EOF1$ (Fig. 3c) exhibits a similar spatial pattern to that of routed river flow (Fig. 3a) while there is about 10–15 cmH_2O anomaly throughout the basin. This indicates that $EOF1$ includes multiple hydraulic components such as discharge on the main stem, river flow on tributaries and soil moisture variations. The similar situation is also true for the 2nd mode: the RMS map of $EOF2$ (Fig. 3d) also shows an evident anomaly along the main stem as well as throughout the basin. This result implies that discharge on the main stem is partly projected into the 2nd mode. This combination of multiple TWS components in the 1st and 2nd EOF modes can be also inferred from $PC1$ and $PC2$ (Fig. 2c). Variations of $PC1$ are comparable to those of river discharge at the Óbidos station, but their phases differ by 1–2 months. This discrepancy leads that $PC1$ does not represent temporal variations of discharge on the main stem. The conclusion here is that conventional EOF decomposition is limited to separate hydraulic components from total water storage.

Because this study aims to extract signal of water mass change from a main stem, additional procedure is required to retrieve the main stem signal from the leading two EOF modes. As an alternative, the VARIMAX method described in Section 2.3 is applied to obtain a signal over the main stem area. TWS variations over the Amazon basin are recovered using the 1st and 2nd modes, and they are transformed into another coordinate system based on a basis rotation. The resulting REOF modes are shown in Fig. 4. The spatial pattern of $REOF1$ (Fig. 4a) and the RMS map from its reconstructed field (Fig. 3e) show a very similar structure to that of the simulated routed river flow (Fig. 3a) without apparent anomaly on tributaries. In addition, the $REOF2$ (Fig. 4b) and the RMS map of its reconstructed field (Fig. 3f) do not show any evident anomaly along the main stem. Consequently, TWS associated with discharge on the main stem and soil moisture variations near the main stem are mostly projected in $REOF1$. Because $REOF1$ includes both river discharges and soil moisture variations that are in-phase with river discharge, its RMS values are higher than those of routed river flow.

The effective separation of water storage signal of main stem is also found in the temporal variation of 1st and 2nd modes of the REOF. Solid red and dashed blue lines in Fig. 4c show the temporal REOF mode 1 and 2 ($RPC1$ and $RPC2$), and solid black line is identical to that of in Fig. 2c. They are normalized similar to Fig. 2c. $RPC1$ agrees remarkably well with the synthetic river discharge at the Óbidos station except for some negative peaks. The slight discrepancies during low water season are likely due to (1) other TWS variations that are not completely separated in the REOF and/or (2) GRACE noise that is particularly problematic in the low-water seasons because the signal to noise ratio is relatively low. Temporal variations of $RPC2$ precede those of $RPC1$ by about two or three months. As shown in Fig. 4b, the $REOF2$ shows a large north-south contrast in anomaly. This dipole spatial pattern and its phase difference compared to water storage signal along the main stem (i.e., discharge) are caused by soil moisture variations between the Southern and Northern basins from GLDAS/Noah and are typical spatio-temporal variations of water storage in the Amazon basin (Marengo, 2005). In addition, $REOF2$ includes river flow on the Solimões

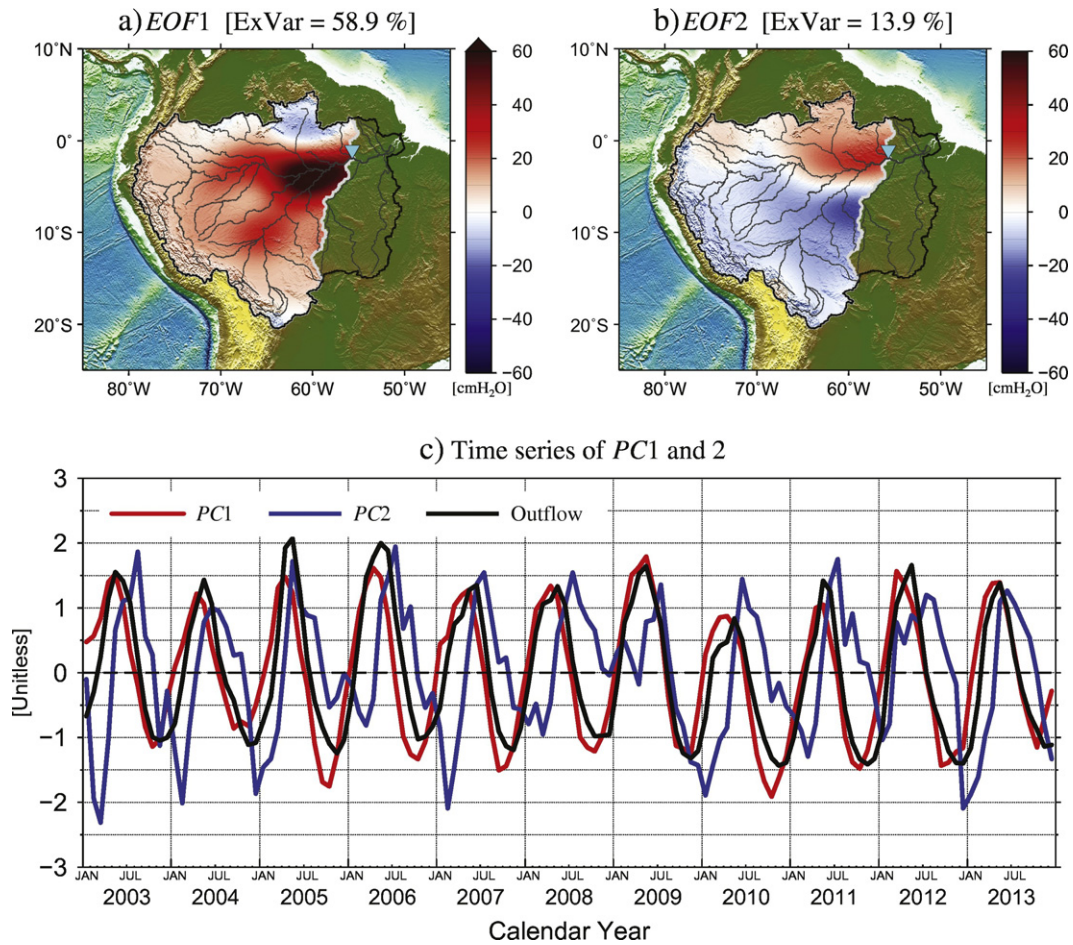


Fig. 2. EOF results for the synthetic GRACE data over the Óbidos sub-basin. (a) The first spatial pattern (*EOF1*) has a strong structure on the main stem. (b) The *EOF2* is characterized by northern-southern dipole pattern; one of them locates on the main stem. The unit for (a) and (b) is cm of equivalent water thickness. (c) shows temporal variations of the normalized first mode (*PC1*, red line) and second mode (*PC2*, blue), and normalized synthetic river discharge at Óbidos station (black line).

River and the Madeira River that was depicted in *EOF1*. As a result, the REOF effectively separates main stem signals from the synthetic data, and thus *RPC1* can be useful to recover river discharge of the basin.

The REOF method can be extended to estimate river discharge for the entire Amazon basin. This is identical to the procedure described above except for sampling GRACE over the entire Amazon basin (represented by thick solid line in Fig. 2) instead of the Óbidos basin. The examination is particularly important because in-situ discharge observation at the outermost mouth of the Amazon basin has been extremely difficult due to the complex river bathymetry and the seawater intrusion (Kosuth et al., 2000). Red line of Fig. 5 shows temporal variations of the 1st REOF on the synthetic GRACE data (*RPC1*) for the entire Amazon basin. Black line exhibits simulated river discharge variations at the basin mouth. Similar to the synthetic test for the Óbidos basin, the two time series agree remarkably well with each other during the study period. This result implies that total river discharge of the Amazon basin, which has not been gauged by an in-situ station, can be determined by the GRACE gravity solutions.

3.2. Recovering river discharge from the real GRACE solutions

As examined with synthetic GRACE data, the REOF method is useful to recover river discharge variations. In this section, the Amazon River discharge is estimated from the real GRACE-REOF method and compared with in-situ discharge data at the Óbidos station. The real

GRACE observations, however, include groundwater effect that the synthetic GRACE data could not depict. Beighley et al. (2009) showed that about 40% of the Amazon TWS is associated with groundwater variations, which is the similar amount compared to the surface water on flood plains and channels. However, its contribution should be very small near the basin outlet: the main stem region (20,700 km²) of the basin only accounts for less than 3% of the entire Amazon area (Sippe et al., 1998), and thus the groundwater contribution along the main stem would be considerably smaller than surface water. Furthermore, as we discussed in the synthetic case, groundwater and other TWS components which are significant over the entire basin can be effectively separated from the river runoff at the main stem via EOF because their spatial correlation and temporal variability differ from each other.

Using the Eq. (2), the gridded real GRACE data over the Óbidos basin is decomposed into EOF modes first. Fig. 6 shows the spatial patterns of the first two modes (*EOF1*–*2*) and their corresponding time series (*PC1*–*2*). The first two modes account for 88.9% of the total variance, about 16% higher than the EV values from the synthetic data. This implies that the real GRACE data may have higher signal to noise ratio than the synthetic GRACE data. The *EOF1* and *EOF2* (Figs. 6a and b, respectively) show very similar spatial patterns to those from the synthetic GRACE data (Fig. 2): *EOF1* exhibits large TWS pattern along the main stem while non-negligible anomaly is apparent over the entire basin, and *EOF2* shows a clear north-south dipole pattern. Their corresponding time series (*PC1* and *PC2* in Fig. 6c) are also very similar to the case of

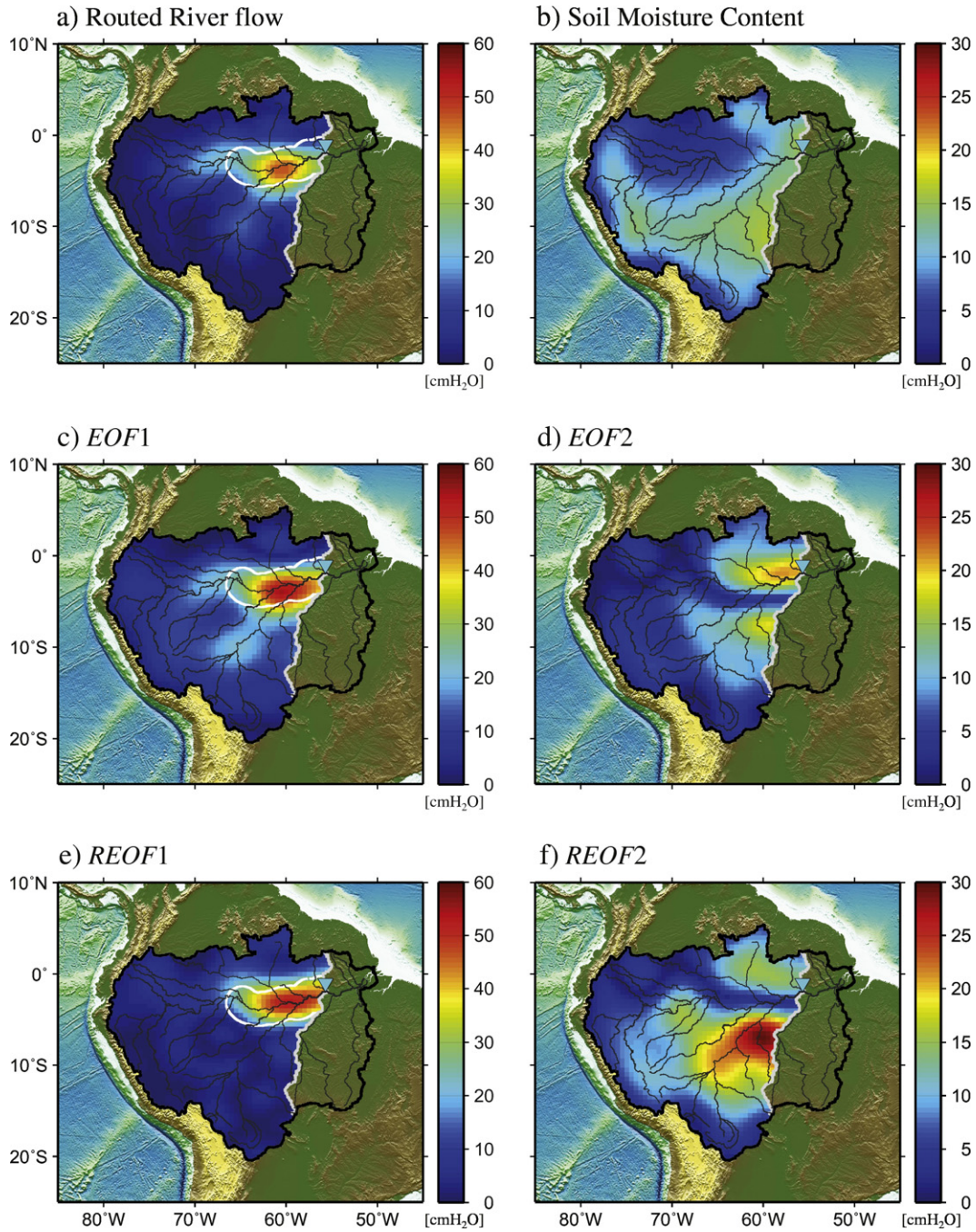


Fig. 3. RMS amplitudes mapped for (a) the simulated the routed river flow and (b) the soil moisture content from GLDAS/CLM, respectively. The routed flow particularly high in main stem while the soil moisture shows strong RMS amplitude in the southern part of the basin. The two maps are smoothed with GRACE spatial resolution for comparing GRACE-EOF results (c-f for EOF1, EOF2, REOF1 and REOF2, respectively). The white line shows the region of main stem.

synthetic GRACE data. Variations of *PC1* (solid red line) are close to those of in-situ river discharge at the Óbidos station while there exists phase difference of one or two months.

Similar to the synthetic GRACE data, the VARIMAX algorithm is used to rotate the leading two modes from the conventional EOF. Fig. 7 shows the resulting REOF modes and it also exhibits similar spatial patterns (*REOF1* and *REOF2* in Figs. 7a and b, respectively) and corresponding time series (*RPC1* and *RPC2* in Fig. 7c) to those of the synthetic data (Fig. 4). *RPC1* (red) shows a similar phase to the in-situ discharge data (black). In particular, negative peaks of *RPC1* exhibit superior agreement with the in-situ data to the case of synthetic test. This is probably due to the signal to noise ratio in real GRACE data higher than that of synthetic GRACE data.

In Fig. 7c, the positive peaks of *RPC1* show apparent deviations from the in-situ data. The most significant difference is found at the 2009 flood, which was called the *once-in-a-century* event in this basin (Marengo et al., 2012). *RPC1* data is consistent with this report while in-situ discharge data at the Óbidos station (black) puts it as the 3rd highest peak in 2003–2013. This discrepancy between the in-situ measurements and the GRACE-REOF estimates is possibly due to the complex floodplain developed during the 2009 flood, which was not accounted for in the ground measurements. While the northern side of the Amazon River at the Óbidos is well confined by the river bank, the opposite side of the river is separated from the Curuaí floodplain (one of the largest floodplain in the basin) merely by a narrow natural levee. When the water level rises in flooding seasons, some part of the

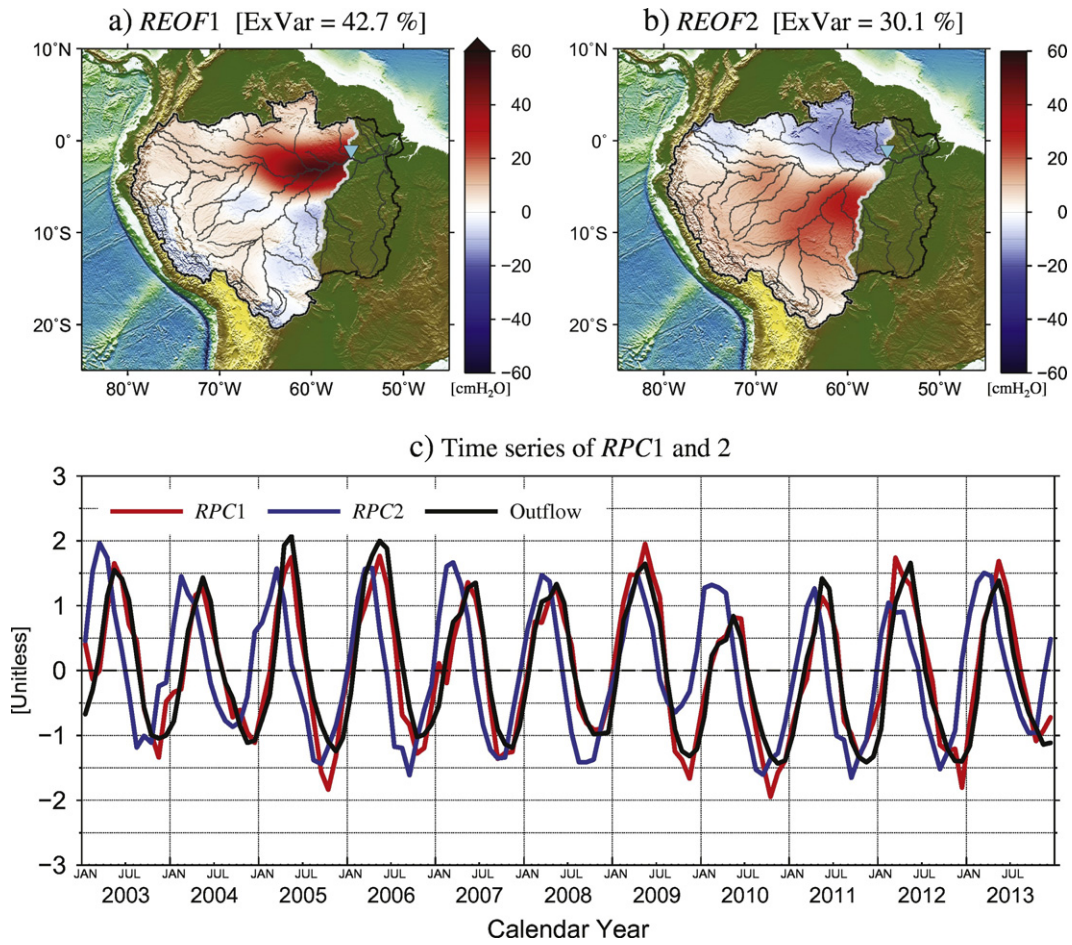


Fig. 4. REOF results for the synthetic GRACE data over the Óbidos sub-basin. Panels here are similar to those in Fig. 2 except that they are yielded from the reconstruction of the two leading EOF modes by rotating basis. *REOF1* (a) is significantly confined in the main stem while *REOF2* (b) has its main structure outside the main stem. (c) shows the temporal patterns of the normalized first mode (*RPC1*, red line) and second mode (*RPC2*, blue). The black line is identical to in Fig. 2(c).

main Óbidos channel can detour the Óbidos station through the Curuaí floodplain forming new flow channels. According to Oltman (1968), the bypassing water volume through the Curuaí varies from 0 to 10% of the total discharge depending on the hydraulic conditions, such as surface water slope and bed roughness of the floodplain. Since the in-situ water level observation is a point measurement from the main river

channel, discharge data obtained in the Óbidos station may differ from the actual water volume during the large flooding events. This possibility is supported by the MODIS imagery captured during the 2009 high-flow season. Fig. 8 compares the MODIS satellite images around the Óbidos station in June 2009 (a) and June 2010 (b), which represent the once-in-a-century (2009) and an ordinary (2010) flooding events,

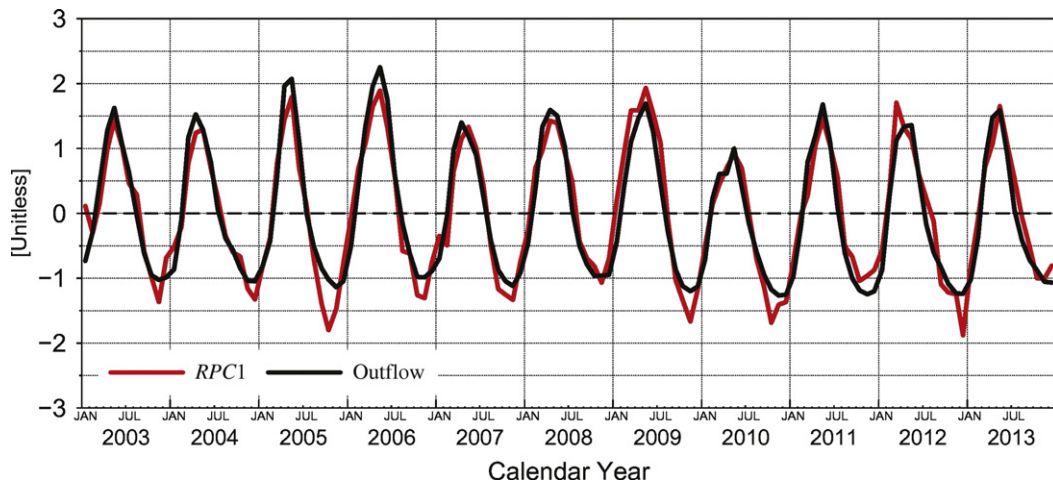


Fig. 5. Comparison between normalized *RPC1* time series (red) and outflow (black) at the basin mouth of Amazon from the synthetic GRACE data. Two time series agrees well with each other.

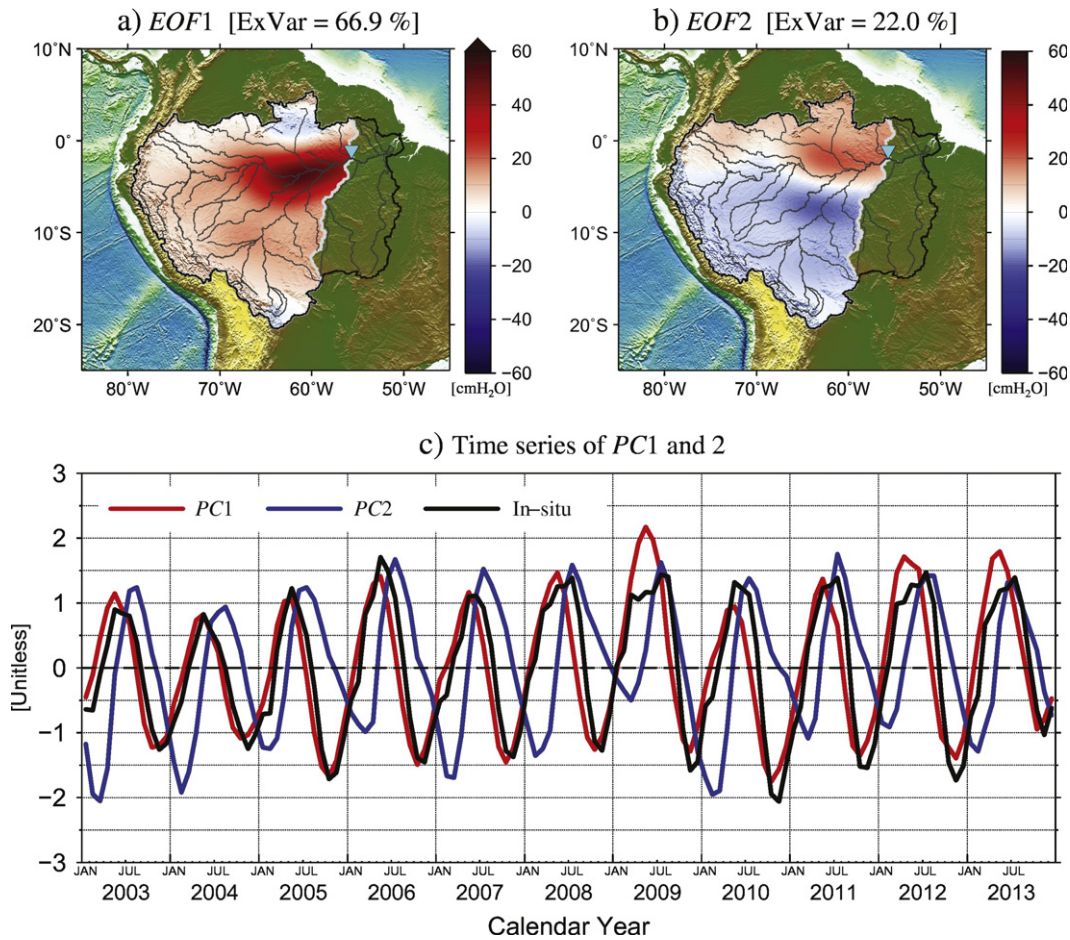


Fig. 6. EOF results for the real GRACE data over the Óbidos sub-basin. (a) The first spatial pattern (*EOF1*) has a strong structure on the main stem. (b) The *EOF2* is also characterized by northern-southern dipole pattern. (a) and (b) are similar to (a) and (b) of Fig. 2, respectively. The unit for (a) and (b) is cm of equivalent water thickness. (c) shows temporal variations of the normalized first mode (*PC1*, red line) and second mode (*PC2*, blue), and normalized in-situ observations at Óbidos station (black line).

respectively. The location of the Óbidos station is marked by cyan triangle. Fig. 8a clearly exhibits wide flow paths in the south, which is not seen in the 2010 flood image. This implies that a large portion of total discharge flowed through the southern floodplain in 2009 may be missed in the in-situ discharge measurements at the Óbidos station. On the other hand, Fig. 8b shows that most of discharge was confined along the main stem. Similar differences between *RPC1* and in-situ data are also shown during flood season in 2012 and 2013, indicating that in-situ observation may underestimate river discharge during flooding.

When using *REOF* derived from the GRACE observation, on the other hand, river discharge is determined over the whole basin with a focus on the main stem area and thus it is not influenced by the local geomorphological variations. This indicates that the GRACE-*REOF* based discharge estimates in 2009 may include the water volume that was missed by the in-situ measurements during the peak flooding season.

Since *RPC1* (red line in Fig. 7c) only shows normalized river discharge, appropriate scaling of *RPC1* is necessary to quantify the volume of discharge in the basin. The *WBE*-based discharge from Eq. (1) (denoted by Q_{WBE} here after) is used to adjust amplitude of the *RPC1*. For precipitation and evaporation, ERA-Interim data (Dee et al., 2011) are used, and the water storage variations are computed from GRACE data. To suppress noise included in the GRACE data, reconstructed data from the first two EOF modes is used. The resulting Q_{WBE} (blue) is additionally shown in Fig. 9. Q_{WBE} has the higher month-to-month variability than those of in-situ data and *RPC1*. The higher variability is likely associated with errors in the reanalysis and GRACE after the first order time-

derivative. However, its overall pattern agrees well with *RPC1* and the in-situ measurement, and thus the Q_{WBE} estimate is useful to auxiliary information for scaling of *RPC1*.

Fig. 10a shows *RPC1* and *WBE* river discharge and the regression between the two. As shown in Fig. 9, Fig. 10a exhibits a similar variation between *WBE* river discharge and *RPC1*. Based on the linear regression, *RPC1*-based river discharge (denoted by Q_{RPC1} here after) can be estimated by adding a mean and scaling amplitude. Fig. 10b exhibits the probability density of the difference between Q_{WBE} and Q_{RPC1} . The probability density in Fig. 10b is associated with misfits between the two that is suspicious of error in Q_{WBE} estimate. The histogram is normally distributed, and thus the higher temporal variations (discrepancy between Q_{RPC1} and Q_{WBE}) are random noise rather than systematic errors. Those results imply that the regression analysis between *RPC1* and Q_{WBE} is reasonably adopted for scaling of *RPC1* data.

With the Q_{RPC1} we can estimate the detouring water mass around the Óbidos station during 2009. Rudorff et al. (2014) estimated that about 2% of the annual discharge detoured around the main channel in the year based on an inundation model. The approach based on GRACE data yields that the 2009 annual discharge from Q_{RPC1} is 6650 Gton, while in-situ discharge is 6250 Gton. The difference is about 6% of annual discharge, and sizable portion of it is likely due to the detouring water flow via the unaccounted floodplain. Fig. 9 shows that discharge discrepancy between in-situ and Q_{RPC1} is apparent since 2008. This is probably because the method for estimating discharge at the station was adjusted to accurately determine water volume passing the channel (Ore-Hybam, personal communication, 2014).

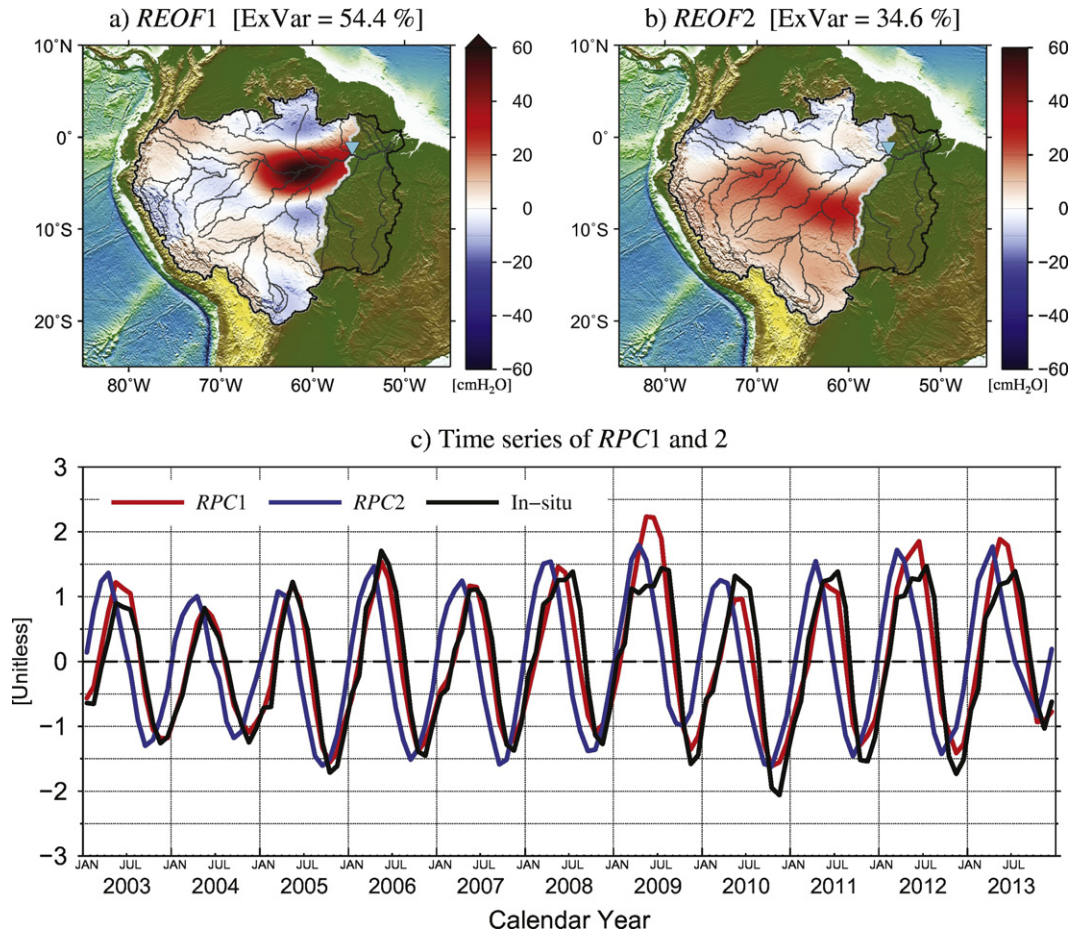


Fig. 7. REOF results for the real GRACE data over the Óbidos sub-basin. *REOF1* (a) is mostly confined in the main stem while *REOF2* (b) has its main structure outside the main stem. Normalized *RPC1* (red in (c)) and *RPC2* (blue in (c)) show temporal variations of *REOF1* and *REOF2*, respectively. In particular, *RPC1* represents temporal variations of water storage along the main stem and its flood plain because its spatial pattern is strongly confined to the main stem. The black line in (c) represents normalized in-situ observations at Óbidos station, identical to that shown in Fig. 6. The red shows the very similar variations to the black line except during high water season.

Uncertainty of the discharge estimate Q_{RPC1} largely originates from two main sources: the GRACE measurement noise and imperfect REOF mode separation between the water mass signal along the main stem and from nearby area. Assuming that most of the measurement noise is smoothed out in the course of the EOF decomposition, negligible error from the noise would remain in Q_{RPC1} . However, imperfect mode separation may result in spurious seasonal to longer-cycle errors of Q_{RPC1} , which would be more dominant in the resulting uncertainty. In order to quantify an approximate range of the uncertainty in Q_{RPC1} , the Óbidos gauge data have been used. The root mean squared

difference (RMSD) between the gauge discharge and Q_{RPC1} is 34.53 Gton/month in September–February (low flow season) and 65.02 Gton/month in March–August (high flow season). The higher uncertainty in March–August is likely contributed by the larger in situ discharge measurement error for high flow events. These separate estimates can be considered as the upper bounds of the Q_{RPC1} uncertainty for low and high flow periods of the study basin.

The novel method introduced in this work can be also extended to the entire Amazon basin. Red line in Fig. 11 shows the total discharge over the entire Amazon basin estimated by the combination of REOF

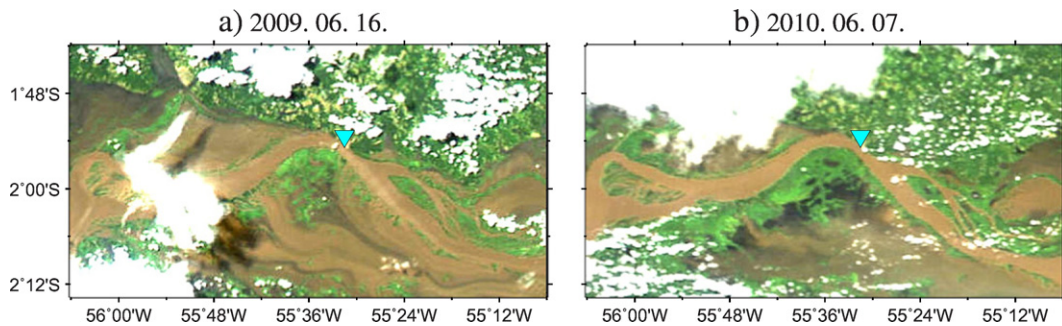


Fig. 8. MODIS satellite images around the Óbidos station in June 2009 (a) and June 2010 (b). The location of the Óbidos station is marked by cyan triangle. The river flows eastward (to right) in this region. (a) clearly exhibits wide flow paths in the south implying a large portion of water volume may be missed in the in-situ discharge measurements at the Óbidos station. (b) shows that most of discharge was confined along the main stem, different with 2009 flood image.

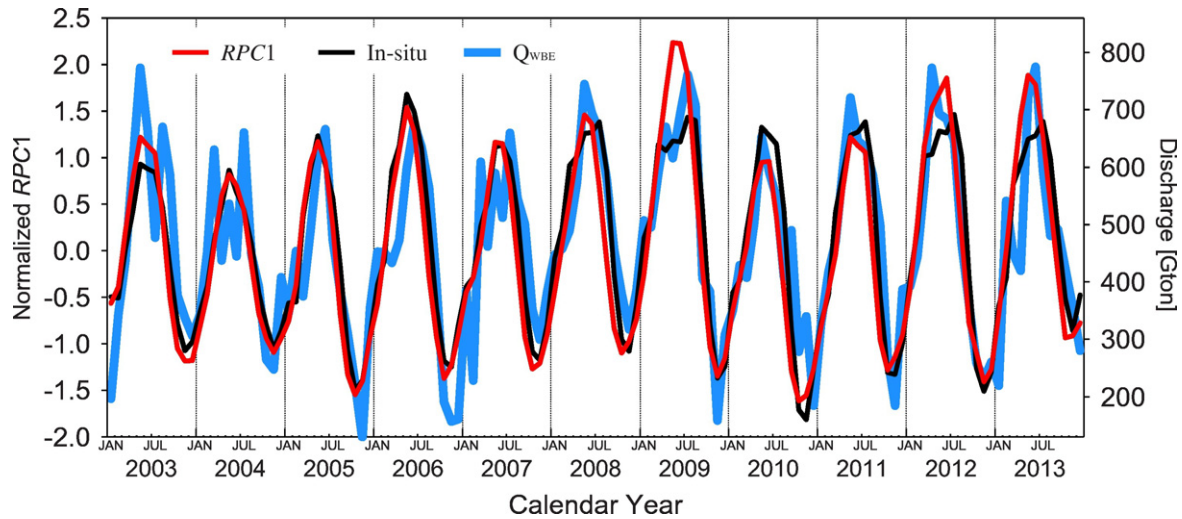


Fig. 9. Comparisons of normalized $RPC1$ with Q_{WBE} and In-situ. Red and black lines are identical to those of (c) in Fig. 7. The blue line representing Q_{WBE} is computed by Eq. (1). Q_{WBE} has the higher month-to-month variability than those of in-situ data and $RPC1$, but its overall pattern agrees with $RPC1$ and the in-situ measurement. This implies that the Q_{WBE} estimate is useful to auxiliary information for scaling of $RPC1$. The right vertical axis represents a physical unit of discharge in Giga-ton ($= 10^{12}$ kg) per month. In-situ discharge is initially recorded in cubic meter per second (m^3/s). To match it with $RPC1$ and Q_{WBE} , we multiply in-situ values by day of month and 86,400 s because $RPC1$ and Q_{WBE} is based on mass observations.

and WBE of GRACE time-varying gravity, and black line shows the discharge over Óbidos basin that is identical to black line in Fig. 8. Fig. 11 shows that the total discharge over Amazon basin is about 23% greater than the Óbidos discharge, and during June 2009, it reached 1050 Gton, which is a unique event exceed 1000 Gton during the study period. Blue line in Fig. 11 represents sum of in-situ discharge from the Óbidos, Itaituba and Altamira stations. The latter two stations are located at two rivers confluent below Óbidos station. The discharge is much closer to red line than that of the Óbidos basin because it incorporates contribution of rest basin outside the Óbidos basin, but it is still smaller than the red line because the three in-situ stations cannot observe net river discharge of the entire Amazon basin. Blue line precedes black and red lines about one month because both additional discharge data are gauged from southern basin, and contribution from northeastern basin is missed because in-situ data is not available at the region.

4. Discussions and conclusions

In this study, we develop a novel method to estimate river discharge over Amazon basin using satellite gravimetric data. TWS recovered from the GRACE gravity solutions are decomposed using the REOF method to extract the signal mainly representing the river discharge along the main channel. To verify the efficacy of the REOF decomposition to estimate the river discharge, we first conduct a synthetic GRACE-REOF experiment using simulated TWS from GLDAS in combination with a simple runoff routing for the realization of river discharge. Estimates of river discharge from the synthetic GRACE-REOF experiment agree well with the synthetic truth discharge at the Óbidos station and the outer-most Amazon River outlet.

The same method is applied to the real GRACE data and its results are compared with in-situ discharge observation at the Óbidos station.

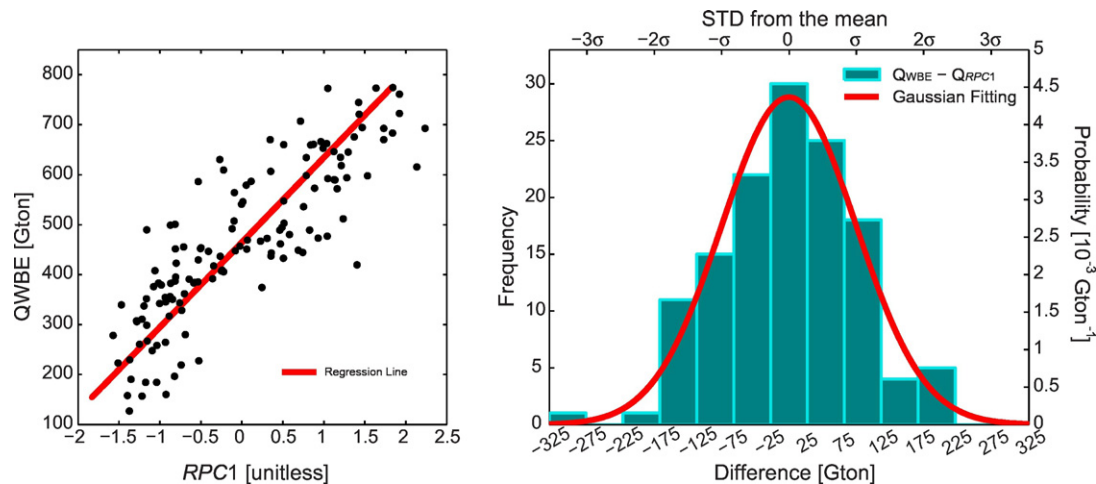


Fig. 10. Results of regression between Q_{WBE} and $RPC1$. (a) $RPC1$ exhibits similar variations to Q_{WBE} . Based on the linear regression, Q_{RPC1} can be estimated by adding a mean and scaling amplitude. (b) shows the probability density of the difference between Q_{WBE} and Q_{RPC1} . The histogram appears normally distributed, and thus the higher temporal variations (discrepancy between Q_{RPC1} and Q_{WBE}) are likely noise.

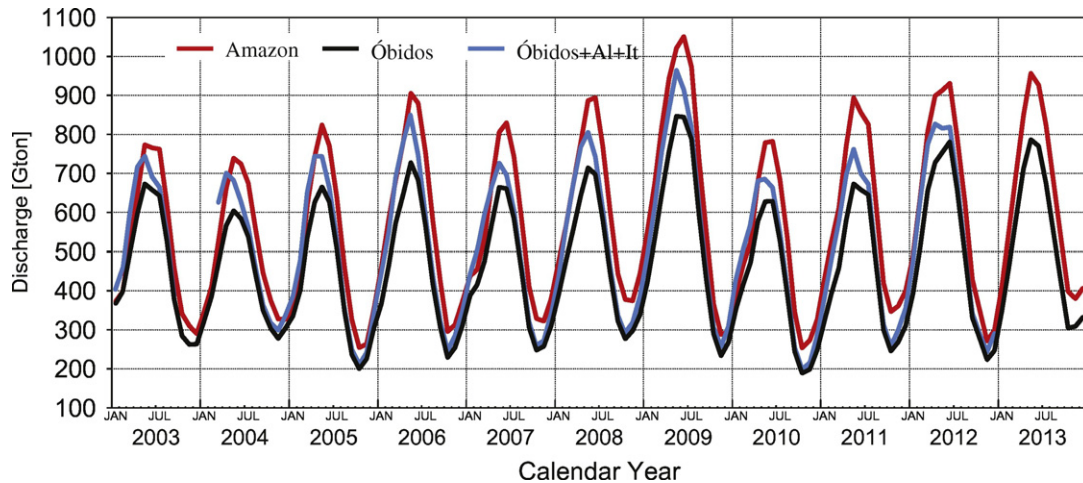


Fig. 11. Estimation of total discharge for the Amazon Basin. Red line shows the total discharge over the entire Amazon Basin estimated by the combination of REOF and WBE of GRACE time-varying gravity. As a comparison, black line shows the discharge over Óbidos basin. The total discharge over Amazon Basin is about 23% greater than the Óbidos discharge. Blue line represents sum of in-situ discharge from the Óbidos, Itaituba and Altamira stations. The latter two stations are located at two rivers confluent below Óbidos station. Like in Fig. 9, physical units of in-situ discharge are converted into monthly outflow mass to compare with discharge based on REOF and WBE.

While the overall time series of the GRACE-REOF and the in-situ discharge values agree remarkably well, they show significant discrepancies for a few high-water seasons. By showing the MODIS image that captures a large-scale detouring of water flows around the gauging station through the Curuaí floodplain, we suggest a possibility that a significant portion of the water volume was missed in the in-situ measurements. This possibility may also be transferrable to the other high-flow seasons. In our analysis, the water mass detouring the station is about 6% of annual discharge of the basin in 2009.

Since the method developed here does not require in-situ observations, it can be extended to the other large basins where in-situ observations are not available at their basin mouths. We estimate discharge of the entire Amazon basin, which was unknown due to complex channel structure and ocean tidal effect. Annual discharge of entire Amazon basin is about 23% greater than that of Óbidos basin, and during the extreme flooding in 2009, it reached 1050 Gton, which is a unique event that exceeds 1000 Gton during the study period.

Our approach can yield monthly river discharge estimates using the monthly GRACE gravity solutions since May 2002. This alternative estimate is particularly important under the decline trend of numbers of gauge stations since 1980's (Shiklomanov et al., 2002). GRACE Follow-On is planned to launch in August 2017 (Flechtner et al., 2014). Therefore, it is expected that space-borne gravity observations can provide multi-decadal variations of river discharge at basin mouths which is highly valuable for assessing the impact of regional or global climate change but has not been possible by in-situ monitoring.

Acknowledgements

This work was supported by National Research Foundation grant NRF-2013R1A1A2008368, Korea Polar Research Institute (KOPRI) research grant PM16020, Korea Meteorological Industry Promotion Agency (KMIPA) research grant KMIPA2015-3033 and Together Science Education for the Future (TOSEF BK 21 PLUS).

References

A. G., Wahr, J., Zhong, S., 2013. Computations of the viscoelastic response of a 3-D compressible Earth to surface loading: an application to Glacial Isostatic Adjustment in Antarctica and Canada. *Geophys. J. Int.* 192, 557–572.

Alsdorf, D.E., Han, S.C., Bates, P., Melack, J., 2010. Seasonal water storage on the Amazon floodplain measured from satellites. *Remote Sens. Environ.* 114, 2448–2456.

Alsdorf, D.E., Lettenmaier, D.P., 2003. Tracking fresh water from space. *Science* 301, 1491–1494.

Alsdorf, D.E., Rodriguez, E., Lettenmaier, D.P., 2007. Measuring surface water from space. *Rev. Geophys.* 45, RG2002.

Beighley, R.E., Eggert, K.G., Dunne, T., He, Y., Gummadi, V., Verdin, K.L., 2009. Simulating hydrologic and hydraulic processes throughout the Amazon River basin. *Hydrol. Process.* 23, 1221–1235.

Bettadpur, S., 2012. CSR Level-2 Processing Standards Document for Level-2 Product Release 05.

Bjerklie, D.M., Lawrence Dingman, S., Vorosmarty, C.J., Bolster, C.H., Congalton, R.G., 2003. Evaluating the potential for measuring river discharge from space. *J. Hydrol.* 278, 17–38.

Cazenave, A., Chen, J., 2010. Time-variable gravity from space and present-day mass redistribution in the Earth system. *Earth Planet. Sci. Lett.* 298, 263–274.

Cheng, M., Tapley, B.D., 2004. Variations in the Earth's oblateness during the past 28 years. *J. Geophys. Res.* 109, B09402.

Dee, D.P., Uppala, S.M., Simmons, A.J., Berrisford, P., Poli, P., Kobayashi, S., Andrae, U., Balmaseda, M.A., Balsamo, G., Bauer, P., Bechtold, P., Beljaars, A.C.M., van de Berg, L., Bidlot, J., Bormann, N., Delsol, C., Dragani, R., Fuentes, M., Geer, A.J., Haimberger, L., Healy, S.B., Hersbach, H., Hólm, E.V., Isaksen, I., Kållberg, P., Köhler, M., Matricardi, M., McNally, A.P., Monge-Sanz, B.M., Morcrette, J.J., Park, B.K., Peubey, C., de Rosnay, P., Tavolato, C., Thépaut, J.N., Vitart, F., 2011. The ERA-Interim reanalysis: configuration and performance of the data assimilation system. *Q. J. R. Meteorol. Soc.* 137, 553–597.

De Paiva, R.C.D., Buarque, D.C., Collischonn, W., Bonnet, M.-P., Frappart, F., Calmant, S., Bulhões Mendes, C.A., 2013. Large-scale hydrologic and hydrodynamic modeling of the Amazon River basin. *Water Resour. Res.* 49, 1226–1243.

Di Baldassarre, G., Claps, P., 2010. A hydraulic study on the applicability of flood rating curves. *Hydrol. Res.* 42, 10–19.

Di Baldassarre, G., Montanari, A., 2009. Uncertainty in river discharge observations: a quantitative analysis. *Hydrol. Earth Syst. Sci.* 13, 913–921.

Espinoza, J.C., Guyot, J.L., Ronchail, J., Cochonneau, G., Filizola, N., Fraizy, P., Labat, D., de Oliveira, E., Ordoñez, J.J., Vauchel, P., 2009. Contrasting regional discharge evolutions in the Amazon basin (1974–2004). *J. Hydrol.* 375, 297–311.

Filizola, N., Latrubesse, E.M., Fraizy, P., Souza, R., Guimarães, V., Guyot, J.L., 2014. Was the 2009 flood the most hazardous or the largest ever recorded in the Amazon? *Geomorphology* 215, 99–105.

Flechtner, F., Morton, P., Watkins, M., Webb, F., 2014. Status of the GRACE Follow-On Mission. In: Marti, U. (Ed.), *Gravity, Geoid and Height Systems: Proceedings of the IAG Symposium GGHS2012, October 9–12, 2012, Venice, Italy*. Springer International Publishing, Cham, pp. 117–121.

Frappart, F., Seoane, L., Ramillien, G., 2013. Validation of GRACE-derived terrestrial water storage from a regional approach over South America. *Remote Sens. Environ.* 137, 69–83.

Getirana, A.C.V., Bonnet, M.-P., Calmant, S., Roux, E., Rotunno Filho, O.C., Mansur, W.J., 2009. Hydrological monitoring of poorly gauged basins based on rainfall-runoff modeling and spatial altimetry. *J. Hydrol.* 379, 205–219.

Gleason, C.J., Smith, L.C., 2014. Toward global mapping of river discharge using satellite images and at-many-stations hydraulic geometry. *Proceedings of the National Academy of Sciences*. 111, pp. 4788–4791.

Han, S.-C., Shum, C.K., Jekeli, C., Kuo, C.-Y., Wilson, C., Seo, K.-W., 2005. Non-isotropic filtering of GRACE temporal gravity for geophysical signal enhancement. *Geophys. J. Int.* 163, 18–25.

Han, S.-C., Kim, H., Yeo, I.-Y., Yeh, P., Oki, T., Seo, K.-W., Alsdorf, D., Luthcke, S.B., 2009. Dynamics of surface water storage in the Amazon inferred from measurements of inter-satellite distance change. *Geophys. Res. Lett.* 36, L09403.

Han, S.-C., Yeo, I.-Y., Alsdorf, D., Bates, P., Boy, J.-P., Kim, H., Oki, T., Rodell, M., 2010. Movement of Amazon surface water from time-variable satellite gravity measurements

- and implications for water cycle parameters in land surface models. *Geochem. Geophys. Geosyst.* 11, Q09007.
- Hannachi, A., Jolliffe, I.T., Stephenson, D.B., 2007. Empirical orthogonal functions and related techniques in atmospheric science: a review. *Int. J. Climatol.* 27, 1119–1152.
- Hersch, R.W., 2009. *Streamflow Measurement*. CRC Press, London.
- IPCC, 2014. *Mitigation of Climate Change. Contribution of Working Group III to the Fifth Assessment Report of the Intergovernmental Panel on Climate Change* (Cambridge, United Kingdom and New York, USA).
- Jalbert, J., Mathevet, T., Favre, A.-C., 2011. Temporal uncertainty estimation of discharges from rating curves using a variographic analysis. *J. Hydrol.* 397, 83–92.
- Jolliffe, I.T., 2002. *Principal component analysis and factor analysis*. *Principal Component Analysis*. Springer, New York, pp. 150–166.
- Klees, R., Revtova, E.A., Gunter, B.C., Ditmar, P., Oudman, E., Winsemius, H.C., Savenije, H.H.G., 2008. The design of an optimal filter for monthly GRACE gravity models. *Geophys. J. Int.* 175, 417–432.
- Knutti, R., Flückiger, J., Stocker, T.F., Timmermann, A., 2004. Strong hemispheric coupling of glacial climate through freshwater discharge and ocean circulation. *Nature* 430, 851–856.
- Kostaschuk, R., Villard, P., Best, J., 2004. Measuring velocity and shear stress over dunes with acoustic Doppler profiler. *J. Hydraul. Eng.* 130, 932–936.
- Kosuth, P., Callède, J., Laraque, A., 2000. Ocean tide waves propagation along downstream Amazon River: measuring the amazon discharge at the estuary. *Building Partnerships*. American Society of Civil Engineers, pp. 1–10.
- Kouraev, A.V., Zakharova, E.A., Samain, O., Mognard, N.M., Cazenave, A., 2004. Ob' river discharge from TOPEX/Poseidon satellite altimetry (1992–2002). *Remote Sens. Environ.* 93, 238–245.
- Lang, M., Pobanz, K., Renard, B., Renouf, E., Sauquet, E., 2010. Extrapolation of rating curves by hydraulic modelling, with application to flood frequency analysis. *Hydrol. Sci. J.* 55, 883–898.
- Leon, J.G., Calmant, S., Seyler, F., Bonnet, M.P., Cauhopé, M., Frappart, F., Filizola, N., Fraizy, P., 2006. Rating curves and estimation of average water depth at the upper Negro River based on satellite altimeter data and modeled discharges. *J. Hydrol.* 328, 481–496.
- Leonard, J., Mietton, M., Najib, H., Gourbesville, P., 2000. Rating curve modelling with Manning's equation to manage instability and improve extrapolation. *Hydrol. Sci. J.* 45, 739–750.
- Longuevergne, L., Scanlon, B.R., Wilson, C.R., 2010. GRACE Hydrological estimates for small basins: evaluating processing approaches on the High Plains Aquifer, USA. *Water Resour. Res.* 46.
- Marengo, J.A., 2005. Characteristics and spatio-temporal variability of the Amazon River Basin Water Budget. *Clim. Dyn.* 24, 11–22.
- Marengo, J.A., Tomasella, J., Soares, W., Alves, L., Nobre, C., 2012. Extreme climatic events in the Amazon basin. *Theor. Appl. Climatol.* 107, 73–85.
- Milly, P.C.D., Wetherald, R.T., Dunne, K.A., Delworth, T.L., 2002. Increasing risk of great floods in a changing climate. *Nature* 415, 514–517.
- Navarra, A., Simoncini, V., 2010. *A Guide to Empirical Orthogonal Functions for Climate Data Analysis*. Springer Science & Business Media.
- Negrel, J., Kosuth, P., 2012. A framework for satellite retrieval of river discharge without in situ measurements. *20 Years of Progress in Radar Altimetry*.
- Nohara, D., Kitoh, A., Hosaka, M., Oki, T., 2006. Impact of climate change on river discharge projected by multimodel ensemble. *J. Hydrometeorol.* 7, 1076–1089.
- Oki, T., Nishimura, T., Dirmeyer, P., 1999. Assessment of annual runoff from land surface models using Total Runoff Integrating Pathways (TRIP). *J. Meteorol. Soc. Jpn. Ser. II* 77, 235–255.
- Oltman, R.E., 1968. *Reconnaissance Investigations of the Discharge and Water Quality of the Amazon River*. US Government Printing Office.
- Petersen-Øverleir, A., Reitan, T., 2009. Accounting for rating curve imprecision in flood frequency analysis using likelihood-based methods. *J. Hydrol.* 366, 89–100.
- Richey, J.E., Nobre, C., Deser, C., 1989. Amazon River discharge and climate variability: 1903 to 1985. *Science* 246, 101–103.
- Riegger, J., Tourian, M.J., 2014. Characterization of runoff-storage relationships by satellite gravimetry and remote sensing. *Water Resour. Res.* 50, 3444–3466.
- Rodell, M., Houser, P.R., Jambor, U., Gottschalk, J., Mitchell, K., Meng, C.J., Arsenault, K., Cosgrove, B., Radakovich, J., Bosilovich, M., Entin, J.K., Walker, J.P., Lohmann, D., Toll, D., 2004. The global land data assimilation system. *Bull. Am. Meteorol. Soc.* 85, 381–394.
- Rudorff, C.M., Melack, J.M., Bates, P.D., 2014. Flooding dynamics on the lower Amazon floodplain: 1. Hydraulic controls on water elevation, inundation extent, and river-floodplain discharge. *Water Resour. Res.* 50, 619–634.
- Schmidt, R., Flechtner, F., Meyer, U., Neumayer, K.H., Dahle, C., König, R., Kusche, J., 2008. Hydrological signals observed by the GRACE satellites. *Surv. Geophys.* 29, 319–334.
- Seo, K.-W., Wilson, C.R., Scambos, T., Kim, B.-M., Waliser, D.E., Tian, B., Kim, B.-H., Eom, J., 2015. Surface mass balance contributions to acceleration of Antarctic ice mass loss during 2003–2013. *J. Geophys. Res. Solid Earth* 120, 3617–3627.
- Seo, K.W., Wilson, C.R., 2005. Simulated estimation of hydrological loads from GRACE. *J. Geod.* 78, 442–456.
- Shabalova, M.V., van Deursen, W.P., Buishand, T.A., 2003. Assessing future discharge of the river Rhine using regional climate model integrations and a hydrological model. *Clim. Res.* 23, 233–246.
- Sheffield, J., Ferguson, C.R., Troy, T.J., Wood, E.F., McCabe, M.F., 2009. Closing the terrestrial water budget from satellite remote sensing. *Geophys. Res. Lett.* 36, L07403.
- Shiklomanov, A.I., Lammers, R.B., Vörösmarty, C.J., 2002. Widespread decline in hydrological monitoring threatens Pan-Arctic Research. *Eos Trans. AGU* 83, 13–17.
- Simpson, M.R., Oltmann, R.N., 1993. *Discharge-measurement System Using an Acoustic Doppler Current Profiler With Applications to Large Rivers and Estuaries*. US Government Printing Office.
- Sippe, S.J., Hamilton, S.K., Melack, J.M., Novo, E.M.M., 1998. Passive microwave observations of inundation area and the area/stage relation in the Amazon River floodplain. *Int. J. Remote Sens.* 19, 3055–3074.
- Smith, L.C., 1997. Satellite remote sensing of river inundation area, stage, and discharge: a review. *Hydrol. Process.* 11, 1427–1439.
- Swenson, S., Wahr, J., 2002. Methods for inferring regional surface-mass anomalies from Gravity Recovery and Climate Experiment (GRACE) measurements of time-variable gravity. *J. Geophys. Res.* 107, 2193.
- Swenson, S., Wahr, J., 2006. Post-processing removal of correlated errors in GRACE data. *Geophys. Res. Lett.* 33, L08402.
- Syed, T.H., Famiglietti, J.S., Chen, J., Rodell, M., Seneviratne, S.I., Viterbo, P., Wilson, C.R., 2005. Total basin discharge for the Amazon and Mississippi River basins from GRACE and a land-atmosphere water balance. *Geophys. Res. Lett.* 32, L24404.
- Tamisiea, M.E., Mitrovica, J.X., Davis, J.L., 2007. GRACE gravity data constrain ancient ice geometries and continental dynamics over Laurentia. *Science* 316, 881–883.
- Velicogna, I., Wahr, J., 2013. Time-variable gravity observations of ice sheet mass balance: precision and limitations of the GRACE satellite data. *Geophys. Res. Lett.* 40, 3055–3063.
- Wahr, J., Molenaar, M., Bryan, F., 1998. Time variability of the Earth's gravity field: hydrological and oceanic effects and their possible detection using GRACE. *J. Geophys. Res.* 103, 30205–30229.
- Wahr, J., Swenson, S., Velicogna, I., 2006. Accuracy of GRACE mass estimates. *Geophys. Res. Lett.* 33, L06401.
- Wouters, B., Schrama, E.J.O., 2007. Improved accuracy of GRACE gravity solutions through empirical orthogonal function filtering of spherical harmonics. *Geophys. Res. Lett.* 34, L23711.
- Xu, K., Zhang, J., Watanabe, M., Sun, C., 2004. Estimating river discharge from very high-resolution satellite data: a case study in the Yangtze River, China. *Hydrol. Process.* 18, 1927–1939.
- Yoon, J.-H., Zeng, N., 2010. An Atlantic influence on Amazon rainfall. *Clim. Dyn.* 34, 249–264.
- Zakharova, E.A., Kouraev, A.V., Cazenave, A., Seyler, F., 2006. Amazon River discharge estimated from TOPEX/Poseidon altimetry. *Compt. Rendus Geosci.* 338, 188–196.
- Zeng, N., Jin-Ho, Y., Jose, A.M., Ajit, S., Carlos, A.N., Annarita, M., Neelin, J.D., 2008. Causes and impacts of the 2005 Amazon drought. *Environ. Res. Lett.* 3, 014002.